Theory of molecular excitation and relaxation near a plasmonic device

Gérard Colas des Francs[a]
Institut Carnot de Bourgogne, CNRS UMR5209, Université de Bourgogne, 9 Avenue A. Savary,
F-21078 Dijon, France

Christian Girard and Thierry Laroche[b]
Centre d'Elaboration de Matériaux et Etudes Structurales (CNRS), Nanoscience Group, 29 rue J. Marvig,
F-31055 Toulouse, France

Gaëtan Lévèque and Olivier J. F. Martin
Nanophotonics and Metrology Laboratory, Swiss Federal Institute of Technology Lausanne (EPFL),
CH-1015 Lausanne, Switzerland

The new optical concepts currently developed in the research field of *plasmonics* can have significant practical applications for integrated optical device miniaturization as well as for molecular sensing applications. Particularly, these new devices can offer interesting opportunities for optical addressing of quantum systems. In this article, we develop a realistic model able to explore the various functionalities of a plasmon device connected to a single fluorescing molecule. We show that this theoretical method provides a useful framework to understand how quantum and plasmonic entities interact in a small area. Thus, the fluorescence signal evolution from excitation control to relaxation control depending on the incident light power is clearly observed. © *2007 American Institute of Physics.* [DOI: 10.1063/1.2748753]

I. INTRODUCTION

The current research stream towards optical system miniaturization is motivated by a need for (i) higher density of integrated photonic components, (ii) low threshold biological and chemical sensors, and (iii) molecular scale characterization of complex biomolecules. In the rapidly growing field of the *nanophotonics*, systems consisting of isolated molecules in interaction with noble metal nanostructures[1,2] are used as prototype models to test and validate new proposal of active plasmonic devices.

In the early stage of the surface molecular spectroscopy, the unusual optical properties of plasmonic materials were already invoked as possible mechanisms for the surface enhanced Raman spectroscopy.[3] Very recently, with the demonstration of the control of fluorescent resonant energy transfer[4] through thin layers of plasmonic materials, a new step towards the *molecular plasmonics* has been achieved.[4–7] These new experiments use the excitation of surface plasmons to enhance and control the efficiency of the light transfer between two remote molecular sites. This control of light transfer in ultrareduced geometry[8,9] could have a positive impact on a future optical technology scalable to molecular dimension.[10] In a closely related context involving the spatial control of sharp metal tips or the effective realization of nanoparticle plasmon waveguides, single molecules are often used as efficient local sensors of the plasmonic near-field intensity.

To support the development of these molecular plas-monic devices, specific theoretical frameworks must be imagined. They should be able to include the complex physics we have to deal with when we couple quantum systems with plasmonic environments. For example, from numerous models, it is well known[11–13] that nanostructured surface samples can dramatically modify the fluorescence lifetime of molecules. However, such information is not sufficient to predict the complete photophysical behavior of the molecule and to determine the amount of energy released by the molecule as a function of both *excitation energy* and the *excitation frequency*. Especially in the presence of plasmonic devices that sustain localized plasmon modes, such an analyzis requires a special attention to properly include local field enhancements, Ohmic losses, and radiative decay rates. In this article, we show that all these characteristics can be included by applying a combination of the *field-susceptibility technique*[13] together with the formalism of the *optical Bloch equations.*[14–17] This self-consistent version of *Maxwell Bloch equation* approach relies on the fact that quantum-mechanical calculations can be restricted to the molecular system,[18] while the complex optical environment can be treated classically using the field-susceptibility technique.

II. LIGHT GUIDING AND CONFINEMENT

To illustrate our technique, we have chosen a system of experimental interest (cf. Fig. 1). In this example, the sample consists of metallic nanoparticles arranged to form plasmonic chain waveguides.[19] Three years ago, direct experimental evidence of short range coupling has been reported by measuring electromagnetic energy transport along silver nanoparticle plasmon waveguides.[19] As described in this reference, the simplest optical method aimed at addressing sur-

---

[a]Electronic mail: gerard.colas-des-francs@u-bourgogne.fr
[b]Present address: LNIO-Université Technologique de Troyes—12, rue Marie Curie BP2060, F10010 Troyes, Cedex, France.
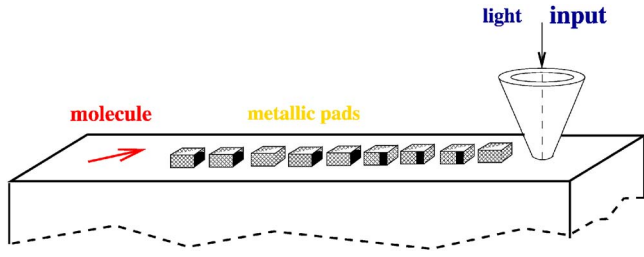
FIG. 1. (Color online) Perspective view of a periodic linear chain of metal particles deposited on a dielectric surface. The chain is optically addressed by the extremity of a SNOM tip. Fluorescent molecules are located at the chain exit.

FIG. 2. (Color online) Optical transmittance of a metal particle chain composed of 15 square shaped gold nanoparticles ($100 \times 100 \times 40 \times$ nm^3) spaced by 100 nm. The arrow inside the inset frame schematizes the SNOM tip dipole orientation: (in blue) the tip dipole is along the longitudinal axis; (in red) the tip dipole is perpendicular to the chain.

face nanostructures consists in using and controlling the light polarization state of the electromagnetic field generated at the apex of the probe tip of a scanning near field optical microscope (SNOM).[20] To describe the excitation electric field, we can assume that the effective tip dipole $\mathbf{m}(t)$, located at $\mathbf{r}_{\text{tip}}$, is driven by an external monochromatic excitation of angular frequency ω_0 and polarized in a direction $\mathbf{a}$ parallel to the surface. It thus oscillates according to the simple cosine law

$$\mathbf{m}(t) = \mathbf{a}m \cos(\omega_0 t). \tag{1}$$

The total near-field distribution $\mathcal{E}(\mathbf{r}, t)$ generated by the SNOM tip around the plasmonic device can be easily obtained by solving a dyadic integral equation

$$\mathcal{E}(\mathbf{r}, t) = \tfrac{1}{2}\{\mathcal{E}(\mathbf{r}, \omega_0)\exp(i\omega_0 t) + \text{c.c.}\} \tag{2}$$

with

$$\mathcal{E}(\mathbf{r}, \omega_0) = \mathcal{S}(\mathbf{r}, \mathbf{r}_{\text{tip}}, \omega_0) \cdot \mathbf{a}m \tag{3}$$

where $\mathcal{S}$ is the total field-susceptibility dyadic tensor of the plasmonic device. This tensor obeys Dyson's equation

$$\mathcal{S}(\mathbf{r}, \mathbf{r}_{\text{tip}}, \omega_0)$$
$$= \mathbf{S}(\mathbf{r}, \mathbf{r}_{\text{tip}}, \omega_0) + \int_{\text{metal}} \mathcal{S}(\mathbf{r}, \mathbf{r}, \omega_0) \cdot \chi(\omega_0) \cdot \mathbf{S}(\mathbf{r}', \mathbf{r}, \omega_0)d\mathbf{r}'. \tag{4}$$

In this relation, $\mathbf{S}$ is the field-susceptibility associated with the bare dielectric surface and $\chi(\omega_0)$ represents the susceptibility of the metal. Equation (4) can be solved numerically by using an algorithm based on a three-dimensional meshing of the metal chain.[13] The electric field around the system is then used to compute at the chain exit (i.e., in a predefined location $\mathbf{R}_m$) near-field transmission spectra

$$I_{\text{chain}}(\mathbf{R}_m, \omega_0) = |\mathcal{E}(\mathbf{R}_m, \omega_0)|^2. \tag{5}$$

When the SNOM tip optically addresses one of the extremities of the chain, the evanescent electric field that tails off the very tip couples with the closest metal post so that significant energy transfer can be triggered along the chain. In Fig. 2, we present transmittance spectra of a gold nanoparticle chain. The transmittance bands correspond to the coupling of localized plasmon modes sustained by each gold pad (located around 620 nm for an isolated gold pad). More p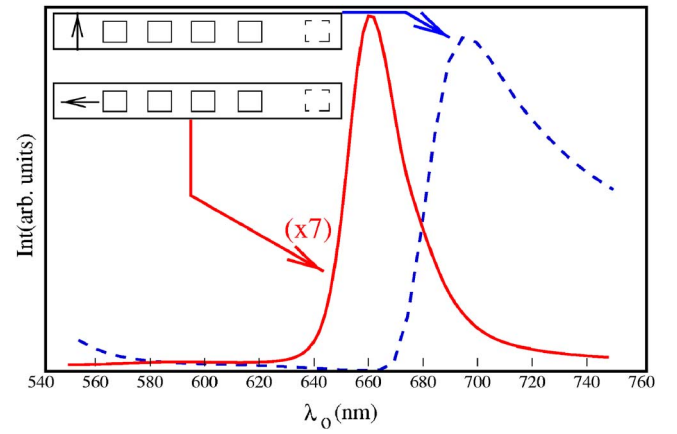recisely, they result from the superimposition of these individual resonances that are redshifted by their mutual interactions. To complete our analysis, we present in Fig. 3 two electric intensity field maps computed around the chain for two wavelengths corresponding to the two maxima of Fig. 2. The guiding efficiency is significantly improved when the extremity of the chain is excited by a transverse electric field [see map (A) of Fig. 3]. Furthermore, in this case the transmittance band (see Fig. 2) is sufficiently broad to address a large family of dye molecules with excitation spectra ranging from 680 to 750 nm. Consequently, in the following of this paper we will use this polarization mode.

III. MOLECULAR FLUORESCENCE

Let us consider a molecular system located at the position $\mathbf{R}_m$ of the chain exit [Fig. 4(a)]. In order to simplify the description, the fluorescing molecule will be schematized by a two-level quantum system characterized by its ground state $|g\rangle$ and its excited state $|e\rangle$ so that $\delta_L = \omega_0 - \omega_e$ is the detuning factor between the laser frequency ω_0 and the resonant molecular absorption frequency ω_e.

The matrix density operator ρ is introduced to describe the molecule dynamics. We define $u = \text{Re}(\rho_{ge}e^{-i\omega_0 t})$, $v = \text{Im}(\rho_{ge}e^{-i\omega_0 t})$, and $w = (\rho_{ee} - \rho_{gg})/2$ the usual Bloch vector. The optical Bloch equations are then written in the rotating wave approximation

$$\dot{u} = \delta_L v - \Gamma_e(\mathbf{R}_m)u/2, \tag{6}$$

$$\dot{v} = -\delta_L u - \Omega(\mathbf{R}_m)w - \Gamma_e(\mathbf{R}_m)v/2, \tag{7}$$

$$\dot{w} = \Omega(\mathbf{R}_m)v - \Gamma_e(\mathbf{R}_m)w - \Gamma_e(\mathbf{R}_m)/2, \tag{8}$$

where we have introduced the Rabi frequency $\Omega(\mathbf{R}_m) = -|\mathbf{P}_{eg} \cdot \mathcal{E}(\mathbf{R}_m, \omega_0)|/\hbar$ and the decay rate $\Gamma_e(\mathbf{R}_m)$, which both depend on the molecule position near the metallic structures. According to Fermi's golden rule and applying the fluctuation-dissipation theorem, this total decay rate is known to depend on the orientation $\mathbf{b}$ of the transition moment P_{eg} of the molecule with the relation[14]

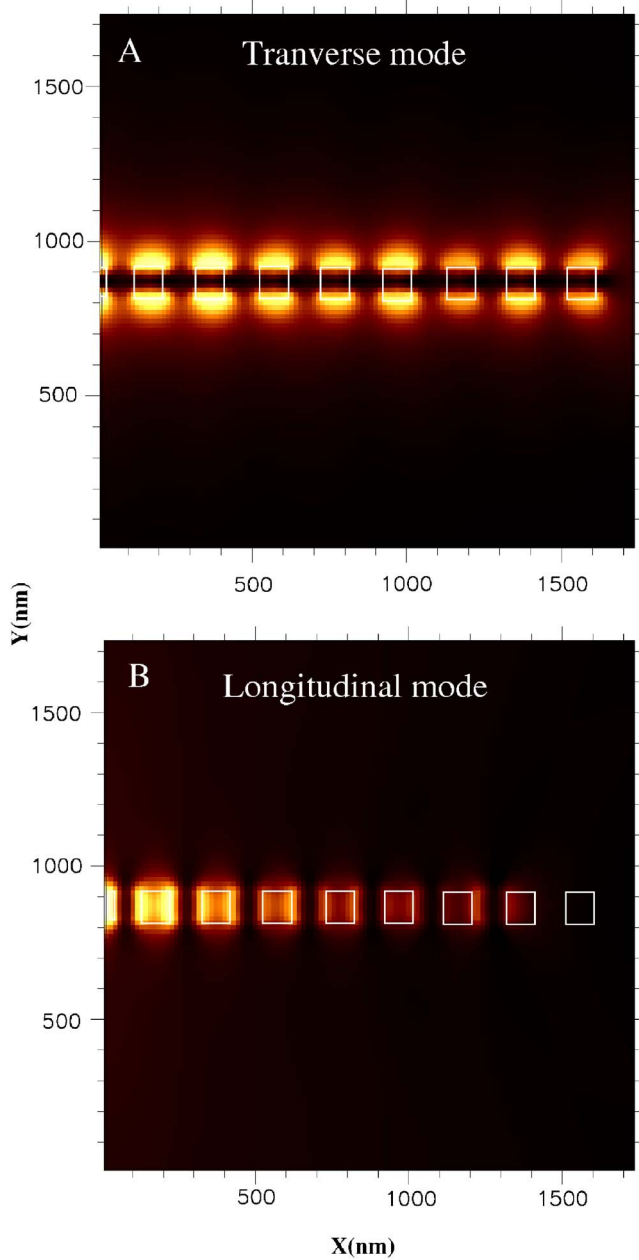**Tranverse mode**

Longitudinal mode

FIG. 3. (Color online) Two near-field optical images along the gold particle chain. The images have been calculated for two polarization modes: (A) transverse mode ($\lambda = 690$ nm) and (B) longitudinal mode ($\lambda = 668$ nm). Color scale increasing from dark brown to bright yellow.

$$\Gamma_e(\mathbf{R}_m) = \Gamma_e^{(0)} + \frac{2P_{eg}^2}{\hbar}\, \mathrm{Im}\{\mathcal{S}(\mathbf{R}_m, \mathbf{R}_m, \omega_e)\}{:}\mathbf{bb}. \quad (9)$$

Note that the field susceptibility that enters the decay rate is nothing but the tensor already introduced to define the electric field in Eqs. (2)–(4). Within this numerical scheme, the fluorescence rate and the excitation field are simultaneously obtained by solving the same Dyson equation (4). Additionally, the complex polarization of the electric near field responsible for the molecular excitation is naturally introduced in the Rabi frequency through the $\mathcal{S}$ dyadic tensor. Finally, it is worthwhile to note that both dissipation and radiative fluorescence relaxation channels are included in the decay rate expression.[21] Figures 4(b) and 5 represent, respectively, the
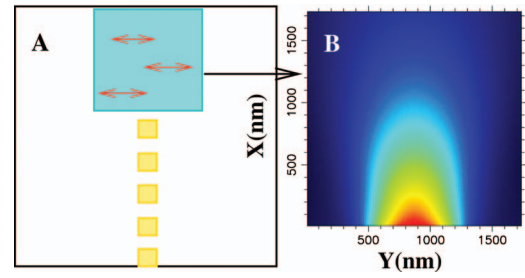

FIG. 4. (Color) (A) Geometry of the molecular addressing area. The molecules deposited in this area lie at 1 nm from the dielectric surface supporting the gold structures. (B) Map of the square modulus of the Rabi frequency $|\Omega(\mathbf{R}_m)|^2$ computed in the addressing area defined in (A). The used wavelength $\lambda_0 = 690$ nm corresponds to the peak of the transverse mode and the transition dipolar moment of the molecule is perpendicular to the chain (see orientation of the red arrows). Rainbow color scale increasing from blue to red.

square modulus of the Rabi frequency Ω^2 and the molecular decay rate Γ_e computed when the molecule is successively oriented along (OX) and (OY) directions. A close look at these three maps indicates the striking difference between excitation light distribution and decay rate topography. For instance, typical local density of states (LDOS) oscillations are observed when moving away from the plasmonic waveguide. These are attributed to the interferences between the fields emitted by the source and reflected by the structure in the classical driven dipole model of the decay rate. In quantum description, node(antinode) of LDOS simply reveals no(good) coupling of the emitted photon to the electromagnetic modes supported by the sample.

The stationary population of the molecule levels can be deduced from the three equations [Eqs. (6)–(8)]. For the excited state we obtain

$$\rho_{ee}(\mathbf{R}_m) = \frac{\Omega^2(\mathbf{R}_m)/4}{\delta_L^2 + \Gamma_e(\mathbf{R}_m)^2/4 + \Omega^2(\mathbf{R}_m)/2}. \quad (10)$$

As indicated by Eq. (10), the molecular population rate ρ_{ee} intricately depends on both Rabi frequency and excited state decay rate. This population coefficient enters the effective signal delivered by the molecule (expressed in energy per time unit) as follows:

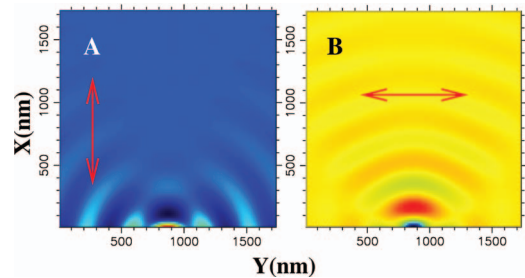$$I_{\mathrm{mol}}(\mathbf{R}_m) = \rho_{ee}(\mathbf{R}_m)\hbar\omega_e\Gamma_e(\mathbf{R}_m). \quad (11)$$

FIG. 5. (Color) Sequence of two maps of molecular decay rate (fluorescing wavelength $\lambda_e = 690$ nm) computed in the green area depicted in the device of Fig. 4(a). In these simulations this quantity has been normalized with respect to the natural linewidth $\Gamma_e^{(0)}$. (A) The molecule is aligned along the (OX) direction; (B) same as (A) along the (OY) direction. Rainbow color scale increasing from blue to red.
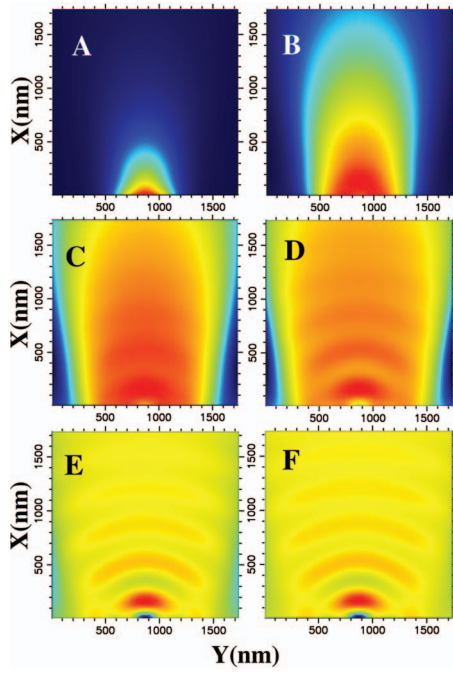
FIG. 6. (Color) Sequence of six maps that describe the evolution of the expected molecule signal when increasing gradually the laser intensity used to address the plasmonic waveguide (fluorescing wavelength $\lambda_e = 690$ nm). These signals have been computed in the green area depicted in the device of Fig. 4(a). (A) Off-saturation absorption regime: Rabi frequency $|\Omega|$ = 100 MHz; (B) $|\Omega| = 500$ MHz; (C) $|\Omega| = 1$ GHz; (D) $|\Omega| = 1.5$ GHz; (E) $|\Omega| = 2$ GHz; (F) $|\Omega| = 2.5$ GHz. Rainbow color scale increasing from blue to red.

(i)   In the limit case, where we work at low Rabi frequency, these relations clearly indicate that the molecule probes the local near-field intensity $|\mathcal{E}_\mathbf{b}(\mathbf{R}_m, \omega_0)|^2$ in the direction (**b**) of its transition dipole moment.

(ii)   In the general case described by Eqs. (10) and (11), the saturated absorption regime occurs when increasing the square modulus of the Rabi frequency beyond the magnitude of $\Gamma_e(\mathbf{R}_m)^2$. The appearance of this phenomenon has been simulated in Fig. 6 by gradually increasing the applied field amplitude. These simulations of the power delivered by the molecule are based on the complete numerical implementation of the *Maxwell-Bloch equations* [Eqs. (2), (4), and (9)–(11)]. The detuning factor has been put to zero and we have fixed the linewidth Γ_0 at 1 GHz. In Fig. 6, we begin the sequence with two maps labeled (A) and (B) in which the Rabi frequency is weaker than the linewidth. In this regime, the molecule essentially responds to the optical near-field intensity that exits the plasmon device. A profound change of the molecule signal occurs when the Rabi frequency range goes beyond the critical value $|\Omega| = 1$ GHz. In this case, the molecule tends progressively to deliver a signal proportional to the LDOS tailored by the plasmonic device itself. For example, in maps (E) and (F) of Fig. 6, the saturation regime is reached and the molecule analyzes the *partial* LDOS (Ref. 22) along the (OY) axis [see the comparison between Figs. 5(b)
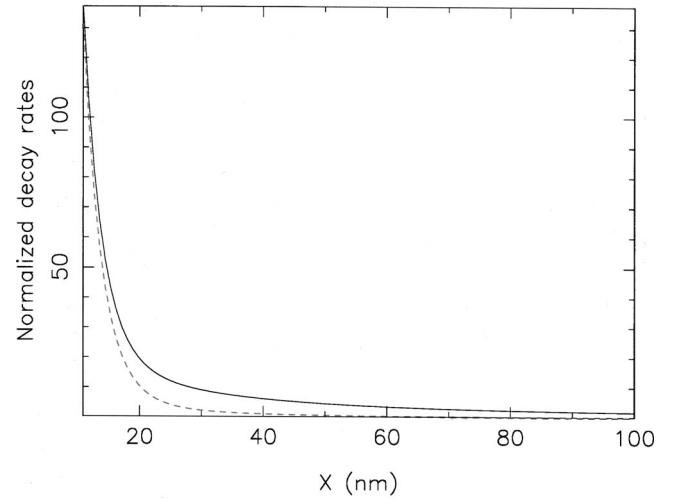

FIG. 7. Normalized total Γ_e (solid line) and nonradiative Γ_{NR} (dashed line) decay rate for molecule at distance X from the last gold pad. The molecule is oriented along the Y axis and is located 1 nm above the substrate.

and 6(f)]. In this case, the molecule looses the history of the successive absorption events and emits fluorescence photons that probe the *partial* LDOS associated with the environment. Such experimental conditions can be obtained by working at low temperature in order to minimize the absorption linewidth Γ_e of the molecular probe. Very recently, Michaelis *et al.* succeeded in operating a low temperature SNOM configuration where the source of light was reduced to a single fluorescing terrylene molecule embedded in a paraterphenyl microcrystal, which itself was glued on the apex of a sharpened optical fiber.[23] These authors have recorded signals related to the variation of the local density of photon states tailored by aluminum surface patterns.

(iii) The fluorescence signal actually detected is the emitted signal [Eq. (11)] minus the power dissipated inside the metallic particles. The dissipated rate is also easily obtained within the field-susceptibility formalism as[24]

$$\Gamma_{NR}(\mathbf{R}_m) = \frac{8}{\hbar} \, \text{Im} \, \chi \int_{\text{metal}} |\mathcal{S}(\mathbf{R}_m, \mathbf{R}_m, \omega_e) \cdot P_{eg}|^2. \quad (12)$$

This nonradiative contribution to the total decay rate is represented on Fig. 7. Near the metal, the decay rate is dominated by Joule losses responsible for quenching but the dissipation becomes negligible above 40 nm. In the case of low temperature conditions as discussed above, this term remains small even at short distances so that the evolution described on Fig. 6 remains valid for the recorded signal.

IV. CONCLUSION

In conclusion, we have developed a unified formalism to describe molecular photophysical processes triggered by complex plasmonic devices. This approach includes a non-perturbative treatment of the excitation field so that large

field enhancement of plasmonic system is naturally taken into account. The generalization to a many level molecular system can be made without any formal difficulty and the method can be easily adapted to other experimental configurations of the nano-optics world (metal tips, apertures, multilayer environment, etc.). Finally, photon counting statistics might be properly treated by applying the generalization of optical Bloch equations recently proposed by Zheng and Brown.[17]

ACKNOWLEDGMENTS

[1] P. Anger, P. Bharadwaj, and L. Novotny, Phys. Rev. Lett. **96**, 113002 (2006).

[2] S. Kühn, U. Hakanson, L. Rogobete, and V. Sandoghdar, Phys. Rev. Lett. **97**, 017402 (2006).

[3] H. Metiu, Prog. Surf. Sci. **17**, 153 (1984).

[4] P. Andrew and W. Barnes, Science **306**, 1002 (2004).

[5] R. V. Duyne, Science **306**, 985 (2004).

[6] A. V. Krasavina and N. I. Zheludev, Appl. Phys. Lett. **84**, 1416 (2004).

[7] P. Mühlschlegel, H.-J. Eisler, O. J. F. Martin, B. Hecht, and D. W. Pohl, Science **308**, 1607 (2005).

[8] H. Ditlbacher, A. Hohenau, D. Wagner, U. Kreibig, M. Rogers, F. Hofer, F. R. Aussenegg, and J. R. Krenn, Phys. Rev. Lett. **95**, 257403 (2005).

[9] C. Girard, E. Dujardin, M. Li, and S. Mann, Phys. Rev. Lett. **97**, 100801 (2006).

[10] M. Sukharev and T. Seideman, J. Chem. Phys. **124**, 144207 (2006).

[11] G. S. Agarwal, Phys. Rev. A **12**, 1475 (1975).

[12] C. Henkel and V. Sandoghdar, Opt. Commun. **158**, 250 (1998).

[13] C. Girard, O. J. F. Martin, G. Lévèque, G. Colas des Francs, and A. Dereux, Chem. Phys. Lett. **404**, 44 (2005).

[14] C. Cohen-Tannoudji, J. Dupont-Roc, and G. Grynberg, *Processus d'Interaction entre Photons et Atomes* (InterEditions, Paris, 1988).

[15] C. M. Bowden and J. P. Dowling, Phys. Rev. A **47**, 1247 (1993).

[16] J. Weiner and P. T. Ho, *Light-Matter Interaction: Fundamentals and Applications*, 1st ed. (Wiley, Hoboken, NJ, 2003), Vol. 1.

[17] Y. Zheng and F. Brown, Phys. Rev. Lett. **90**, 238305 (2003).

[18] D. E. Chang, A. S. Sorensen, P. R. Hemmer, and M. D. Lukin, Phys. Rev. Lett. **97**, 053002 (2006).

[19] S. A. Maier, P. G. Kik, H. A. Atwater, S. Meltzer, E. Harel, B. E. Koel, and A. A. G. Requicha, Nat. Mater. **2**, 229 (2003).

[20] M. Brun, A. Drezet, H. Mariette, N. Chevalier, J. C. Woehl, and S. Huant, Europhys. Lett. **64**, 634 (2003).

[21] P. de Vries, D. V. van Coeverden, and A. Lagendijk, Rev. Mod. Phys. **70**, 447 (1998).

[22] Definition and measurement of *partial* LDOS are discussed in A. Dereux, C. Girard, C. Chicanne, G. Colas des Francs, T. David, E. Bourillot, Y. Lacroute, and J.-C. Weeber, Nanotechnology **14**, 935 (2003).

[23] J. Michaelis, J. M. C. Hettich, and V. Sandogdhar, Nature (London) **405**, 325 (2000).

[24] G. Colas des Francs, C. Girard, M. Juan, and A. Dereux, J. Chem. Phys. **123**, 174709 (2005).